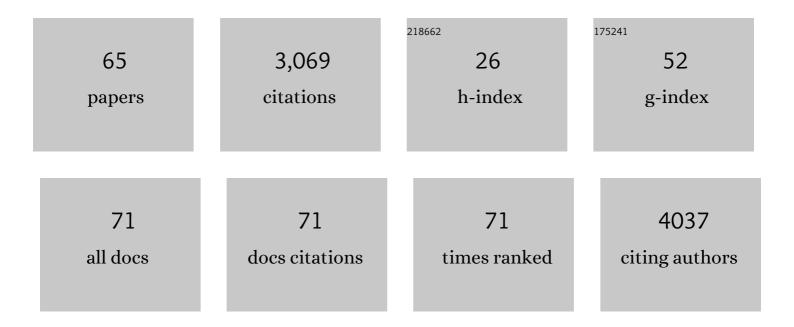
## **Philipp Schneider**

List of Publications by Year in descending order

Source: https://exaly.com/author-pdf/1196662/publications.pdf Version: 2024-02-01



#	Article	IF	CITATIONS
1	Noninvasive 3D Methods for the Study of Dental Cementum. , 2022, , 258-272.		0
2	Quantifying intracortical bone microstructure: A critical appraisal of 2D and 3D approaches for assessing vascular canals and osteocyte lacunae. Journal of Anatomy, 2021, 238, 653-668.	1.5	10
3	3D cyclorama for digital unrolling and visualisation of deformed tubes. Scientific Reports, 2021, 11, 14672.	3.3	2
4	Characterization of the Developing Lacunocanalicular Network During Fracture Repair. JBMR Plus, 2021, 5, e10525.	2.7	6
5	New spinosaurids from the Wessex Formation (Early Cretaceous, UK) and the European origins of Spinosauridae. Scientific Reports, 2021, 11, 19340.	3.3	22
6	Immunofluorescence-guided segmentation of three-dimensional features in micro-computed tomography datasets of human lung tissue. Royal Society Open Science, 2021, 8, 211067.	2.4	3
7	A robust, semi-automated approach for counting cementum increments imaged with synchrotron X-ray computed tomography. PLoS ONE, 2021, 16, e0249743.	2.5	8
8	Imaging techniques for observing laminar geometry in the feather shaft cortex. Journal of Microscopy, 2020, 277, 154-159.	1.8	4
9	Development of protocols for the first serial block-face scanning electron microscopy (SBF SEM) studies of bone tissue. Bone, 2020, 131, 115107.	2.9	24
10	Reptile-like physiology in Early Jurassic stem-mammals. Nature Communications, 2020, 11, 5121.	12.8	30
11	A highly pneumatic middle Cretaceous theropod from the British Lower Greensand. Papers in Palaeontology, 2020, 6, 661-679.	1.5	6
12	Synchrotron radiation-based X-ray tomography reveals life history in primate cementum incrementation. Journal of the Royal Society Interface, 2020, 17, 20200538.	3.4	9
13	3D mapping of blood vessel networks and cells in COPD and non-COPD lung tissue samples using micro-computed tomography and immunofluorescence. , 2020, , .		0
14	Regulation of the Bone Vascular Network is Sexually Dimorphic. Journal of Bone and Mineral Research, 2019, 34, 2117-2132.	2.8	19
15	X-ray Micro-Computed Tomography for Nondestructive Three-Dimensional (3D) X-ray Histology. American Journal of Pathology, 2019, 189, 1608-1620.	3.8	57
16	Regional diversity in the murine cortical vascular network is revealed by synchrotron X-ray tomography and is amplified with age. , 2018, 35, 281-299.		15
17	An Automated Step-Wise Micro-Compression Device for 3D Dynamic Image-Guided Failure Assessment of Bone Tissue on a Microstructural Level Using Time-Lapsed Tomography. Frontiers in Materials, 2018, 5, .	2.4	10
18	Small-angle X-ray scattering tensor tomography: model of the three-dimensional reciprocal-space map, reconstruction algorithm and angular sampling requirements. Acta Crystallographica Section A: Foundations and Advances, 2018, 74, 12-24.	0.1	46

PHILIPP SCHNEIDER

#	Article	IF	CITATIONS
19	Image-based modelling of skeletal muscle oxygenation. Journal of the Royal Society Interface, 2017, 14, 20160992.	3.4	13
20	Nanoindentation analysis of the micromechanical anisotropy in mouse cortical bone. Royal Society Open Science, 2017, 4, 160971.	2.4	32
21	Phase contrast synchrotron radiation computed tomography of muscle spindles in the mouse soleus muscle. Journal of Anatomy, 2017, 230, 859-865.	1.5	17
22	Simultaneous visualisation of calcified bone microstructure and intracortical vasculature using synchrotron X-ray phase contrast-enhanced tomography. Scientific Reports, 2017, 7, 13289.	3.3	31
23	Investigation of microvascular morphological measures for skeletal muscle tissue oxygenation by image-based modelling in three dimensions. Journal of the Royal Society Interface, 2017, 14, 20170635.	3.4	10
24	Soft tissue 3D imaging in the lab through optimised propagation-based phase contrast computed tomography. Optics Express, 2017, 25, 33451.	3.4	10
25	Ultrastructure Organization of Human Trabeculae Assessed by 3D sSAXS and Relation to Bone Microarchitecture. PLoS ONE, 2016, 11, e0159838.	2.5	21
26	Effect of combined treatment with zoledronic acid and parathyroid hormone on mouse bone callus structure and composition. Bone, 2016, 92, 70-78.	2.9	17
27	Techniques to assess bone ultrastructure organization: orientation and arrangement of mineralized collagen fibrils. Journal of the Royal Society Interface, 2016, 13, 20160088.	3.4	104
28	Three-dimensional characterization of fibroblast foci in idiopathic pulmonary fibrosis. JCI Insight, 2016, 1, .	5.0	73
29	High-resolution 3D imaging of osteocytes and computational modelling in mechanobiology: insights on bone development, ageing, health and disease. , 2016, 31, 264-295.		50
30	Combining immunostaining with micro-computed tomography to visualise the 3D distribution of mast cells in idiopathic pulmonary fibrosis. , 2016, , .		0
31	Inverse Finite Element Modeling for Characterization of Local Elastic Properties in Image-Guided Failure Assessment of Human Trabecular Bone. Journal of Biomechanical Engineering, 2015, 137, .	1.3	13
32	Nanostructure surveys of macroscopic specimens by small-angle scattering tensor tomography. Nature, 2015, 527, 349-352.	27.8	170
33	3D scanning SAXS: A novel method for the assessment of bone ultrastructure orientation. Bone, 2015, 71, 42-52.	2.9	61
34	Advanced Glycation End-Products Reduce Collagen Molecular Sliding to Affect Collagen Fibril Damage Mechanisms but Not Stiffness. PLoS ONE, 2014, 9, e110948.	2.5	113
35	Quantitative phenotyping of bone fracture repair: a review. BoneKEy Reports, 2014, 3, 550.	2.7	24
36	Modeling microdamage behavior of cortical bone. Biomechanics and Modeling in Mechanobiology, 2014, 13, 1227-1242.	2.8	23

PHILIPP SCHNEIDER

#	Article	IF	CITATIONS
37	Altered lacunar and vascular porosity in osteogenesis imperfecta mouse bone as revealed by synchrotron tomography contributes to bone fragility. Bone, 2014, 61, 116-124.	2.9	72
38	A quantitative framework for the 3D characterization of the osteocyte lacunar system. Bone, 2013, 57, 142-154.	2.9	95
39	The importance of the intracortical canal network for murine bone mechanics. Bone, 2013, 53, 120-128.	2.9	29
40	Studying osteocytes within their environment. Bone, 2013, 54, 285-295.	2.9	51
41	Imaging of Cellular Spread on a Three-Dimensional Scaffold by Means of a Novel Cell-Labeling Technique for High-Resolution Computed Tomography. Tissue Engineering - Part C: Methods, 2012, 18, 167-175.	2.1	5
42	Deformable image registration and 3D strain mapping for the quantitative assessment of cortical bone microdamage. Journal of the Mechanical Behavior of Biomedical Materials, 2012, 8, 184-193.	3.1	61
43	Serial FIB/SEM imaging for quantitative 3D assessment of the osteocyte lacuno-canalicular network. Bone, 2011, 49, 304-311.	2.9	123
44	The importance of murine cortical bone microstructure for microcrack initiation and propagation. Bone, 2011, 49, 1186-1193.	2.9	41
45	Analysis of sintered polymer scaffolds using concomitant synchrotron computed tomography and in situ mechanical testing. Journal of Materials Science: Materials in Medicine, 2011, 22, 2599-2605.	3.6	30
46	Threeâ€dimensional morphometry of strained bovine periodontal ligament using synchrotron radiationâ€based tomography. Journal of Anatomy, 2010, 217, 126-134.	1.5	10
47	Ptychographic X-ray computed tomography at the nanoscale. Nature, 2010, 467, 436-439.	27.8	766
48	Towards quantitative 3D imaging of the osteocyte lacuno-canalicular network. Bone, 2010, 47, 848-858.	2.9	139
49	Automated, High-Throughput, Multi-scale Assessment of Bone Morphology and Bone Competence. IFMBE Proceedings, 2010, , 841-843.	0.3	0
50	Post-processing technique for improved assessment of hard tissues in the submicrometer domain using local synchrotron radiation-based computed tomography / Nachbearbeitungstechnik für eine verbesserte Erfassung harten Gewebes im Submikrometerbereich mittels lokaler synchrotronstrahlungsbasierter Computertomographie. Biomedizinische Technik, 2009, 54, 48-54.	0.8	12
51	Simultaneous 3D visualization and quantification of murine bone and bone vasculature using microâ€computed tomography and vascular replica. Microscopy Research and Technique, 2009, 72, 690-701.	2.2	58
52	Time-lapsed assessment of microcrack initiation and propagation in murine cortical bone at submicrometer resolution. Bone, 2009, 45, 164-173.	2.9	78
53	MECHANICAL LOADING INDUCES BONE FORMATION AND INCREASED VASCULARIZATION IN CORTICAL BONE. Journal of Biomechanics, 2008, 41, S50.	2.1	0
54	THE INFLUENCE OF THE CORTICAL CANAL NETWORK ON MURINE BONE MECHANICS. Journal of Biomechanics, 2008, 41, S185.	2.1	0

PHILIPP SCHNEIDER

#	Article	IF	CITATIONS
55	INVESTIGATION OF MICRODAMAGE IN MURINE BONE UNDER DYNAMIC LOAD. Journal of Biomechanics, 2008, 41, S76.	2.1	6
56	Synchrotron radiation CT methods for 3D quantitative assessment of mechanically relevant ultrastructural properties in murine bone. Proceedings of SPIE, 2008, , .	0.8	0
57	Preparation and characterization of calibration standards for bone density determination by micro-computed tomography. Analyst, The, 2007, 132, 1040.	3.5	33
58	Ultrastructural Properties in Cortical Bone Vary Greatly in Two Inbred Strains of Mice as Assessed by Synchrotron Light Based Micro- and Nano-CT. Journal of Bone and Mineral Research, 2007, 22, 1557-1570.	2.8	166
59	Hierarchical microimaging for multiscale analysis of large vascular networks. NeuroImage, 2006, 32, 626-636.	4.2	161
60	Functional microimaging: an integrated approach for advanced bone biomechanics and failure analysis. , 2006, , .		1
61	Assessment of murine bone ultrastructure using synchrotron light: towards nano-computed tomography. , 2006, 6318, 86.		1
62	Cellular phenotyping of the mouse skeleton using synchrotron based nano-computed tomography. Journal of Biomechanics, 2006, 39, S448.	2.1	2
63	Phase contrast tomography: An alternative approach. Applied Physics Letters, 2006, 88, 214104.	3.3	62
64	Hierarchical bioimaging and quantification of vasculature in disease models using corrosion casts and microcomputed tomography. , 2004, , .		2
65	Soft-tissue and phase-contrast imaging at the Swiss Light Source. , 2004, , .		2